Electronic Supplementary Material (ESI) for Soft Matter.

Supporting Information

Biopolymer-Supramolecular Polymer Hybrids for Photocatalytic Hydrogen Production

*Jacob E. Kupferberg, Zois Syrgiannis, Luka Đorđević, Eric P. Bruckner, Tyler J. Jaynes, Hakim Ha, Evan Qi, Kristen S. Wek, Adam J. Dannenhoffer, Nicholas A. Sather, H. Christopher Fry, Liam C. Palmer, Samuel I. Stupp**

Experimental Methods:

Catalyst Synthesis and Loading: ($(NH_4)_2(Mo_3S_{13})$ (Catalyst **1**) was synthesized using the method from Kibsgaard et al.[1]. 7.692 mL of ammonium sulfide was added to a round bottom flask followed by the addition of 0.5 g of elemental sulfur (S_8). The solution was sonicated to yield a bright orange solution. In a separate vial, 1 g of $(NH_4)_6Mo_7O_{24}*4H_2O$ was dissolved in 5.1 mL of deionized water, then added to the sulfur solution, to yield a dark red solution. The flask was then firmly sealed to avoid evaporation and heated for 5 days at 90°C using an oil bath to yield dark red crystals. After 5 days, the crystals were filtered, washed with water and then ethanol. The crystals were then transferred to a flask with 100 mL of toluene, brought to a boil, and allowed to boil for 1 hour to dissolve residual sulfur. The crystals were filtered, washed with 200 mL of fresh toluene, then dried under vacuum overnight. The crystals were stored under Ar in a -20°C freezer when not in use. A stock solution of catalyst **1** was made by putting a known mass of catalyst into a glass vial, adding deionized water to the vial, and dissolving with drops of 4 M NaOH to yield a light brown to brown-red solution (depending on the concentration). Samples were sonicated to ensure full dissolution. Samples containing catalyst **1** were loaded with catalyst to achieve a concentration of 36 µM of catalyst (36 nmol per mL).

$Mo_3S_7(S_2C_3NH_6)_3I$ (Catalyst **2**) was synthesized using a method from Fontenot et al.[2]. 0.305 g of Catalyst **1** and 0.307 g of tetramethylthiuram disulfide were added to a round bottomed flask with a stir bar. Then anhydrous N,N-dimethylformamide (20 mL) was added to the flask, sealed under N_2, stirred at ambient temperature for 30 minutes, then heated to 50°C. An excess of ethanolic NaI solution (2 g NaI in 50 mL of absolute ethanol) was added to the DMF solution and stirred for two more hours at 50°C. The reaction vessel was cooled to room temperature after two hours, and the bright orange precipitate was collected by vacuum filtration, washed with ethanol, and then washed with diethyl ether. Samples were then added to a small volume dichloromethane, boiled to create a supersaturated solution, then allowed to cool to room temperature to induce crystallization. Catalyst solution was created by adding catalyst **2** to dimethyl sulfoxide (DMSO). A few drops of aqueous 4M NaOH was added to the DMSO solution to induce full catalyst solubility. The solution was then filtered through a 0.45 µm PTFE filter to remove excess NaOH precipitates. Samples containing catalyst **2** were loaded to achieve a concentration of 36 µM of catalyst.

$(Mo_3S_4(H_2O)_9)Cl_4$ (Catalyst **3**) was synthesized using a method from Shibahara et al.[3]. 9 g of $(NH_4)_2MoS_4$ was dissolved in 300 mL of deionized water to create a red solution. 9 g of sodium borohydride in 120 mL of deionized water and 120 mL of 6 M HCl were pipetted alternately (4 mL each) into the $(NH_4)_2MoS_4$ solution under vigorous stirring at room temperature. Then 480 mL of 6 M HCl was added to the resultant dark brown suspension, raised to 90 °C, and bubbled with air for 20 h to produce a green solution. Additional 1 M HCl solution was added to the flask if the total volume was less than 300 mL. After 20 hours, the solution was cooled using an ice bath and filtered. The precipitate was washed with a small amount of 1 M HCl after which the wash solution was added to the filtered solutions. A rotary evaporator was used to reduce the total volume to 100 mL after which the solution was filtered and passed through a Sephadex G-10 column (diameter 4 cm, length 80 cm), the eluent being 1 M HCl. A small amount (ca. 1%) of $[Mo_3S_3O]^{4+}$ (aq) (green, λ_{max}= 605 nm in 1 M HCl) was followed by the aqua ion 4' (green, λ_{max}= 620 nm in 1 M HC1), which was collected. For concentration and purification, the solution containing the aqua ion $[Mo_3S_4(H_2O)_9]^{4+}$ was diluted to five times its original volume with water and was absorbed on a short Dowex 50W-X2 cation exchanger column (diameter 2 cm, length 15 cm) and eluted with 2 M HCl slowly. The solution was fully dried to yield a green precipitate and then washed with methanol. The solution was then filtered and the precipitate was dried and stored under Ar at -20°C. Samples containing catalyst **3** were loaded to achieve a concentration of 360 µM of catalyst.

The synthesis of amorphous MoS_3 nanoparticles followed a procedure by Lee et al.[4]. 0.4 g of $(NH_4)MoS_4$ was added to 100 mL of deionized water to yield a dark red solution. Then 6 mL of concentrated HCl was added slowly under stirring. The suspension was stirred for 30 minutes (or until bubbling ceased) and the resulting dark brown particles were centrifuged out of suspension. The particles were then washed with deionized water and methanol. The particles were then suspended in a small volume of water, frozen with liquid nitrogen, and lyophilized. Solutions of catalyst **4** were made by adding catalyst **4** particles to a deionized water followed by sonicating to ensure total mixing. Samples containing catalyst **4** were loaded to achieve a concentration of 111.6 mg of catalyst per mL (584 µmol per mL assuming a molecular weight of 192.15 grams per mole for MoS_3).

FTIR Characterization of Catalysts: Fourier-transform infrared (FTIR) analysis was performed on solid catalyst using attenuated total reflection (ATR) spectroscopy on a Nexus 870 spectrometer.

X-Ray Diffraction Characterization: X-ray diffraction (XRD) analysis was performed for solid catalyst on a silicon substrate using a benchtop Rigaku Miniflex XRD. The scan rate used was 0.5 degrees per minute with scan steps of 0.005 degrees.

Estimation of SA Ionic Strength: SA is composed of guluronic monomers and mannuronic monomers are epimers with molar mass of 216.12 g/mol for their sodium salt. The monomer is received as a sodium salt and is dispersed in deionized water. Thus, we assume that a 1 wt% (w/w) solution of SA is equivalent to a 46 mM of Na-Carboxylate pairs.

UV-Visible Absorption Spectroscopy: UV-Visible absorption spectroscopy on solutions was performed in a 0.05 mm path length, closed demountable quartz spectrophotometer cell (Starna Cells) using an Ocean Optics QEPro Spectrophotometer equipped with a DH-2000-Bal lamp.

Scanning Electron Microscopy: Hydrogel samples were prepared for SEM using critical point drying (CPD). Hydrogel samples were soaked in deionized water overnight to remove any excess salts. These samples were run through a sequential exchange with aqueous ethanol solutions (25%, 50%, 60%, 70%, 80%, 90%, 95%, 100%) at ten-minute intervals. These solutions were prepared using 200 proof absolute ethanol. Samples were then loaded into microporous polymer capsules with 70 μm pores and run through CPD and a 20-minute purge timer on a Tousimis Samdri-795. Samples were removed and stored under vacuum until measurement.

CPD prepared samples were cleaved to expose cross-section and then adhered to the SEM stub using carbon tape. Samples were coated with 8 nm of osmium (Filgen, OPC-60A) to prevent charging during imaging. All SEM images were taken using a Hitachi SU8030 instrument with an accelerating voltage of 2 kV.

Accounting for Swelling Differences: The simplest method to determine catalyst loading in an individual sample was through the mass of the gel. We assumed that gels were homogeneously mixed. However, different SA loadings can lead to differences in swelling/shrinking upon gelation. These differences in volume will produce inaccurate mass measurements.

A calibration curve was created to more accurately assess the true mass of the gel samples. The curve was created as follows: inks were extruded into a 0.5 M $CaCl_2$ solution and the mass was recorded. SA gel samples were prepared with different SA loadings and extruded from different nozzle diameters. The samples were lightly dried with a Kimwipe prior to weighing to avoid additional mass from adsorbed liquid (the same protocol was followed for photocatalysis measurements). The sample was then massed in a glass vial. The gel was then fully dried at 100^{o}C to determine the mass of the solids contained in the gel. This mass was used to calculate the volume of the original ink. The density of the ink of the ink was calculated under the assumption that the added SA solids do not increase the volume of the solution. The calculated initial volume of the gel was used with the known concentration of catalyst in the ink to calculate the moles of catalyst within the gel sample. These measurements were made in triplicate for each SA loading and for several nozzle diameters. These ratios were then used to determine the actual catalyst loading in each gel sample. See **Fig. S11** for data recorded from this process.

Gas Chromatography Measurement: For H_2 quantification, an aliquot less than 1 mL was taken from the sample vial and injected via autosampler into a gas chromatograph (Shimadzu GC-2014) equipped with a 5 Å molecular sieve column, argon carrier gas, and a thermal conductivity detector. Vials contained some overpressure due to the gas evolution, but we did not consider the pressure buildup in the turnover number (TON) calculation. This discrepancy can lead to underestimation of the TON and the turnover frequency (TOF). Eight-point calibration curves for H_2 and N_2 were created using a standard gas (7% H_2 balanced with N_2) and integrated peak areas were used to determine the H_2 concentration in the sample headspace at STP.

Calculation of Turnover Numbers (TON):

$$TON = \frac{Moles\ of\ H_2 Produced}{Moles\ of\ Catalyst} \quad (1)$$

$$TOF = \frac{TON}{Time\ of\ Irradiation} \quad (2)$$

Moles of H_2 produced are measured as follows: an aliquot of headspace is removed from the photocatalysis vial and measured in the GC via autosampler. The moles of H_2 were calculated using a calibration curve. Based on the volume of headspace injected and the calculated moles of H_2 measured, we determine the concentration of H_2 in the headspace. We then determine using the known headspace volume the total moles of H_2 in the headspace. Based on the low solubility of H_2 in water, it is assumed that there is minimal H_2 present in the aqueous phase of the vial.

Catalyst content within a sample vial was estimated from the mass of the gel put into the vial. PMI-SA ink was gelled with $CaCl_2$ solution, washed with deionized water, then lightly dried of excess water with a Kimwipe prior to weighing in the vial to record the **Measured Mass**. It was determined that during the process of gelation and weighing, some water was lost from the gel. This ratio was calculated for different extrusion diameters and SA loadings and allowed us to calculate the **Original Mass** of the gel from its **Measured Mass**. From the **Original Mass**, we calculated the **Original Volume** based on the density of the original ink. From this **Original Volume** we calculated the **True Moles of Catalyst** present in the gel. The concentration of catalyst is constant within the original ink and it is assumed that minimal catalyst loss occurs during the gelling and weighing steps. This method of measuring catalyst content ensures we accurately calculate the moles of catalyst present in the gel regardless of the volume changes experienced. Calculating catalyst content from the **Measured Mass** would underrepresent the amount of catalyst, which would give an overestimate of TON.

H_2O_2 Measurement: H_2O_2 was measured using a colorimetric enzyme assay. Briefly, 1.7 mg of horseradish peroxidase (HRP) was added to 50 mL of deionized water containing 1 tablet of sodium citrate phosphate buffer to produce a final concentration of 50 mM buffer at pH 5.0. A separate stock solution of tetramethylbenzidine (TMB) was made by adding 1 mg of TMB to 1 mL of DMSO. For each H_2O_2 measurement, 20 μL of TMB stock solution and 3 mL of HRP stock

solution were added to a 1 cm path length quartz cuvette and mixed to homogeneity. The sample solution was added to the cuvette, well mixed, and then the 650 nm peak was measured. The H_2O_2 concentration was calculated using a calibration curve. Faradaic efficiency was estimated using the current passed during chronoamperometry (2 e^- for each H_2O_2) and the measured moles of H_2O_2.

Hydrogel Conductivity Measurements: Hydrogel discs of a defined thickness and diameter, typically 1.0 mm thick and 9.0 mm diameter, were synthesized and soaked in deionized water overnight. The gels were then sandwiched using clips between two cleaned FTO substrates using a silicone spacer to control the through gel distance. The remaining space was backfilled with deionized water. For the fully compressed samples no electrolyte was added and no spacer was used, so it was assumed that the spacing distance was the thickness of the compressed gel (about 0.075 mm). In chronoamperometry measurements, a voltage bias of 0 V or -0.3 V was applied across the hydrogel and the current was measured until stabilized to minimize contribution from ionic conductivity. Electrochemical impedance spectroscopy (EIS) measurements were made by applying a bias of -0.3 V with an oscillation magnitude of 5 mV at an oscillation frequency that decreased from 100000 Hz to 1 Hz. Most measurements were made under both dark and illuminated conditions using 5000K White Light LED at 300 mA current.

Electrode Preparation: Electrode substrates used were FTO coated glass with a compact NiO blocking layer. The process was based off of methods from Ho et al[5]. FTO coated glass was cleaned by sonicating for 15 minutes in water with Alconox detergent, reagent ethanol, and methanol. The FTO was then dried using N_2 stream. Prior to spin coating, substrates were UV-Ozone treated for 15 minutes to remove any contaminants and ensure good wettability. Nickel (II) acetate in methoxyethanol (0.5 M) was deposited on cleaned FTO glass at 2000 RPM for 30 s with 2 s ramp time. This deposition was repeated a second time. The electrodes were then sintered at 450 °C under air for 30 min to create a dense layer of NiO apparent as a transparent gray film on the electrode.

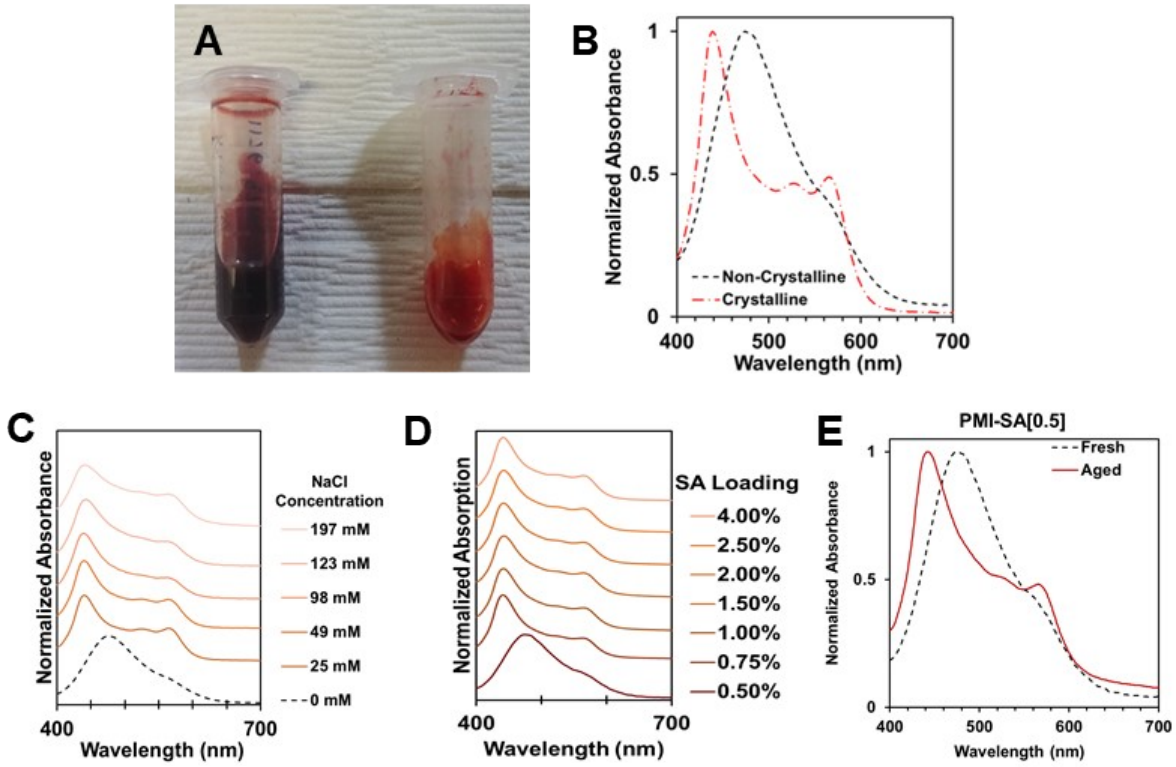

Fig. S1. (A) Photograph of (left) dark red solution of 9.6 mM PMI in deionized water and (right) bright red solution of 9.6 mM PMI in 50 mM NaCl solution. (B) UV-vis absorption spectra of 9.6 mM PMI samples from image S2A, corresponding to the crystalline and non-crystalline states, respectively, as described previously[6-7]. (C) UV-vis absorption spectra of 9.6 mM PMI at various NaCl concentrations. PMI crystallinity is induced at all salt concentrations tested, corroborating previous studies (D) UV-vis absorption spectra of freshly prepared 9.6 mM PMI in various loadings of SA.[19] SA loading above 0.75 wt% induces crystallinity in PMI, but does not seem to affect the absorption behavior beyond changes in scattering. (E) However, PMI crystallinity is not apparent at 0.5 wt% SA after mixing [Fresh], despite occurring at an equivalent ionic strength solution of NaCl (25 mM). However, after one day of ageing [Aged] PMI-SA at 0.5 wt% SA displayed typical crystalline absorption. It is proposed that the increased viscosity of the SA slowed the assembly of PMI at this lower ionic strength.

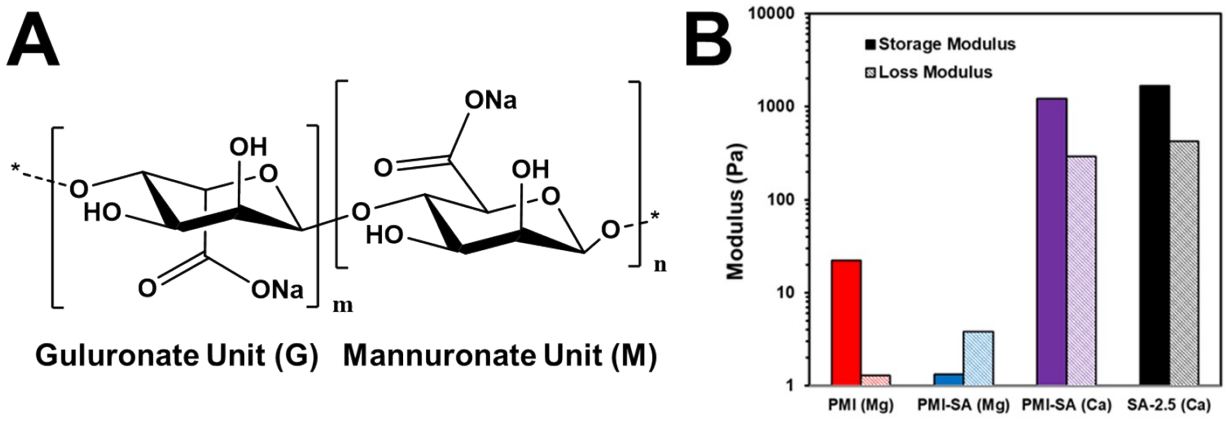

Fig. S2. (A) Molecular structure of the guluronate unit (G) and the mannuronate unit (M) monomers that make up SA. (B) Measurements were made using small amplitude oscillatory shear on a CP-25 fixture. Storage and loss moduli of PMI and PMI-SA samples crosslinked with 50 mM of divalent cation. PMI-NaCl is composed of 9.6 mM PMI and 50 mM NaCl and PMI-SA is composed of 9.6 mM PMI and 2.5 wt% SA. Samples noted (Mg) were gelled *in situ* with 50 mM $MgCl_2$ and samples noted (Ca) were gelled *in situ* with 50 mM $CaCl_2$. Mg^{2+} does not gel SA but can gel PMI. The fact that PMI-SA (Mg) does not reach gel strength similar to PMI-SA (Ca) indicates that PMI-PMI gelation does not contribute strongly to the final gel structure. In addition, the similar strength of PMI-SA (Ca) and SA (Ca) indicate that the mechanical properties of fully gelled PMI-SA arise primarily from SA.

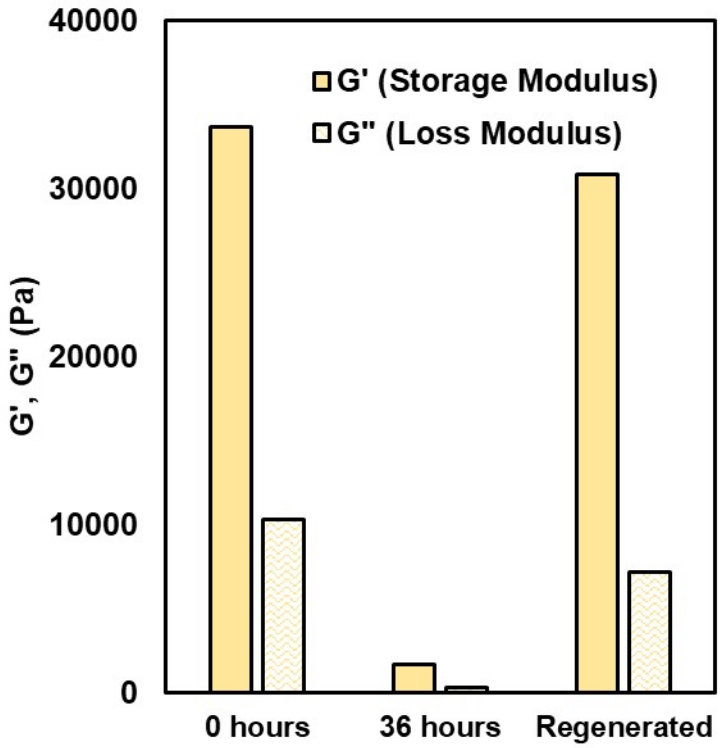

Fig. S3. Rheology of an SA[2.5] gel disc soaked in AA catalysis solution for 36 hours. Over the course of 36 hours of soaking, the SA gel significantly softened due to loss of Ca^{2+} ions. Soaking the gel in 0.5 M $CaCl_2$ solution after soaking in AA solution returned the gel to similar viscoelastic strength (Regenerated), indicating that gel dissolution is occurring through ion exchange rather than polymer degradation. The addition of 160 mM $CaCl_2$ to the AA solution maintained the original gel viscoelasticity over 36 hours.

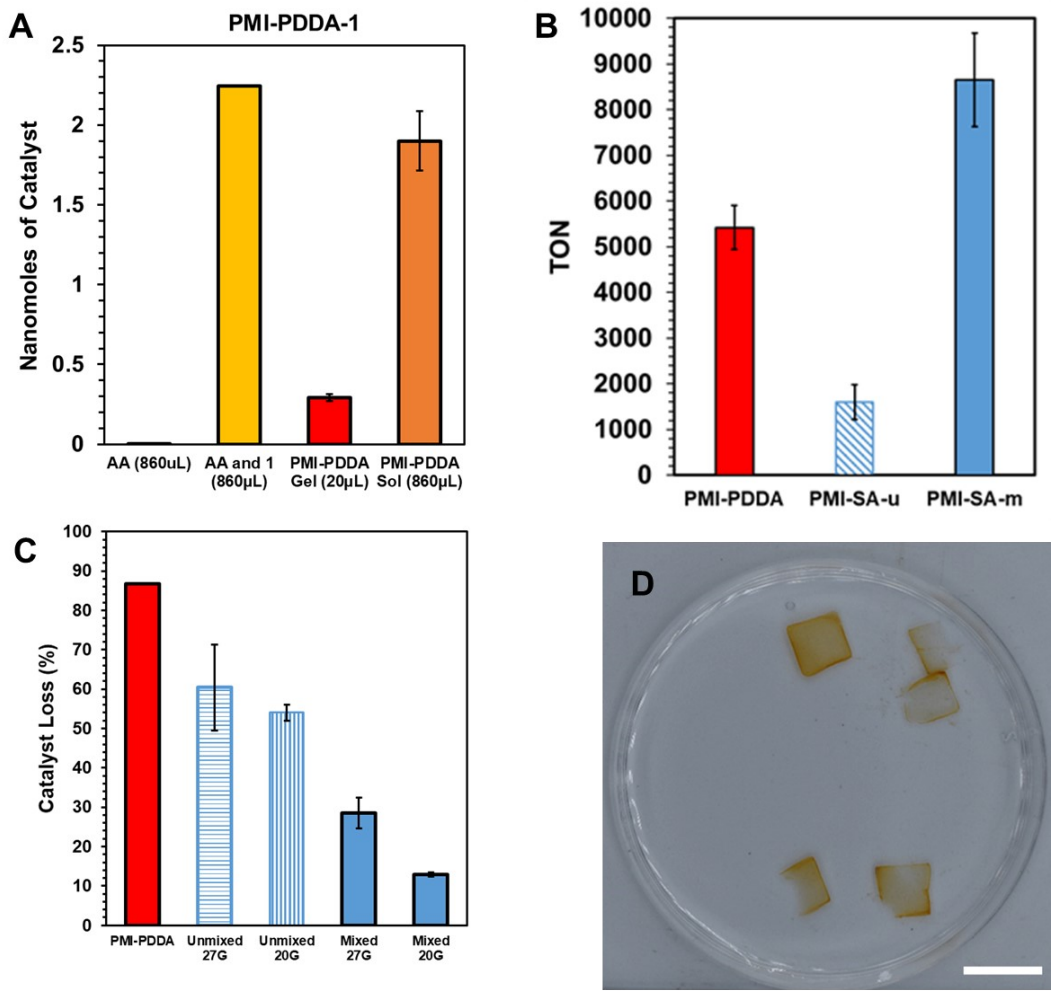

Fig. S4. (A) ICPMS of analysis for Mo of different components of the PMI-PDDA photocatalysis system. PMI-PDDA was prepared as in previous studies with catalyst **1** and the individual components were analyzed after 18 hours of photocatalysis. The PMI-PDDA hydrogel was separated from the catalysis solution by centrifugation and dispersed in a small amount of catalysis solution for removal. **AA** is 860 µL of as-prepared AA solution, **AA and 1** is 840 µL of as-prepared AA solution with 20 µL of added catalyst **1** solution (1 mg/7.5 mL), **PMI-PDDA Gel** is the centrifuged PMI-PDDA hydrogel dispersed in 20 µL of catalysis solution, and **PMI-PDDA Sol** is 860 µL of the remaining catalysis solution separated from the PMI-PDDA hydrogel. The combined catalyst content of the PMI-PDDA gel and the surrounding AA solution add up to the original AA and catalyst solution. In addition, when the volume of added sample is accounted for, the PMI-PDDA Gel and PMI-PDDA Sol had a similar concentration of catalyst **1**, indicating that the gel does not aggregate the catalyst in any meaningful way. (B) TON of PMI-

PDDA and PMI-SA samples using catalyst **1**. PMI-SA-u represents the unmixed sample and PMI-SA-m represents the mixed sample. Both gels were extruded using a 27G nozzle diameter (C) Estimate of catalyst lost to the surrounding AA solution during 18 hours of photocatalysis determined by ICPMS of catalysis solution. (D) Photograph of **SA[3]** gel soaked in a solution of **1** (1 mg/7.5 mL) and sliced (scale bar = 1 cm). The gel (roughly a cube with 0.75 cm per side) was allowed to soak overnight in water and was then sliced with a razor blade to reveal an inhomogeneous distribution of catalyst **1**, which has a distinct brown color. Thicker samples, featured at the top of the Petri dish, displayed a light brown hue in the gel interior, indicating that some catalyst did penetrate the gel surface. However, cutting the gel into a thinner slice reveals that the color is more the product of gel thickness than catalyst concentration.

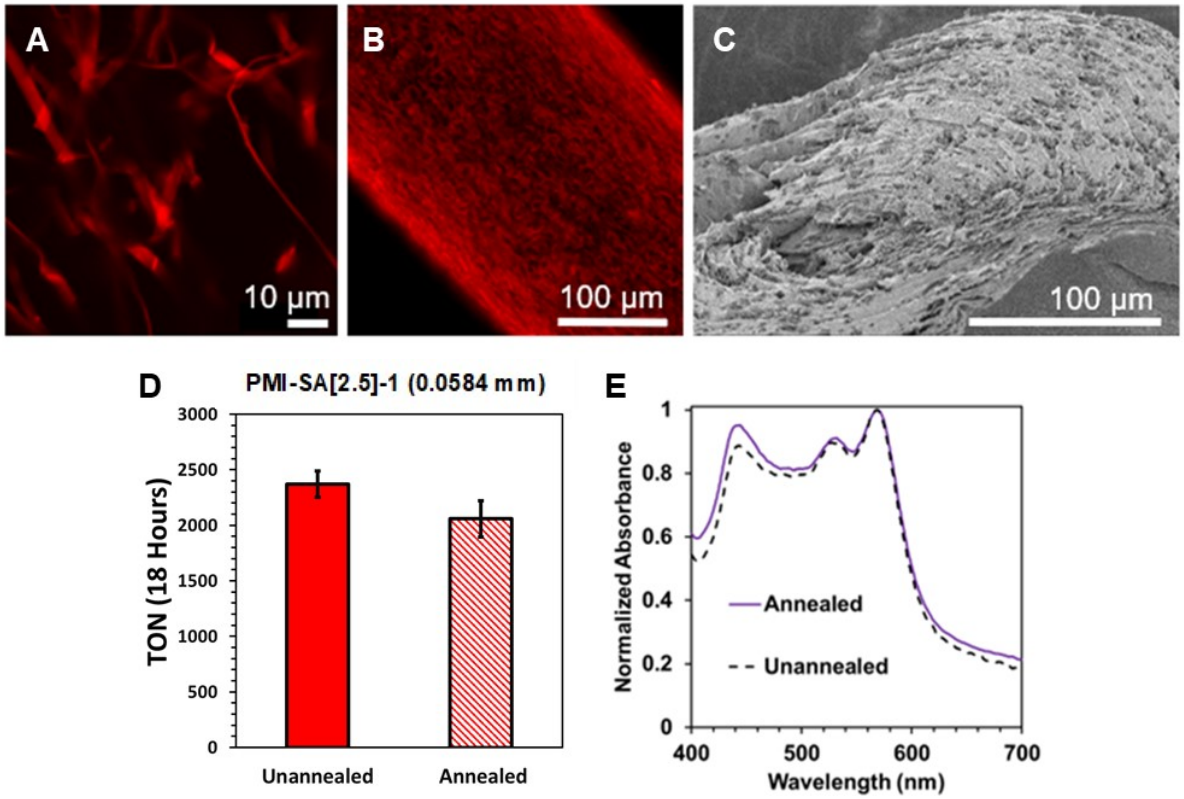

Fig. S5. (A) Confocal microscopy image of PMI (red) in 2.5 wt% SA after being annealed. Annealing process was based previous study[8]. (B) Confocal micrograph of PMI-SA[2.5] gel made with annealed PMI-SA[2.5]. Large ribbons are visible, with larger thickness apparent. (C) SEM cross-sectional image of PMI-SA[2.5] gel made from annealed PMI-SA. Large pores are visible and attributed to the growth and presence of large PMI ribbons. (D) TON for HER of hydrogels made from annealed and unannealed PMI-SA[2.5]. (E) UV-vis spectra of annealed PMI-SA[2.5] and unannealed PMI-SA[2.5]. The slightly altered absorption spectra are attributed to scattering and stacking of the PMI ribbons. Updated methods yielded PMI-SA[2.5] with the typical absorption spectra.

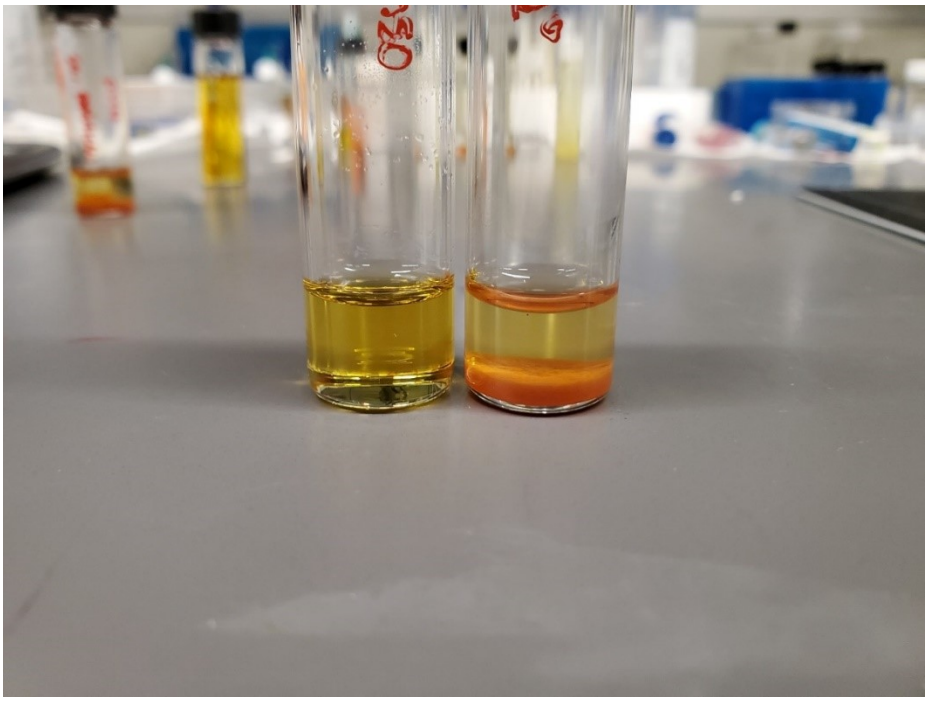

Fig. S6. Photograph of catalyst **2** in different solution conditions. Initial catalyst **2** solution was 1.4 mg/mL of catalyst **2** in DMSO with a few drops of 4 M NaOH. The left vial is a 1:1 (v/v) mixture of catalyst **2** and DMSO. The right vial contains a 1:1 (v/v) catalyst **2** solution and deionized water. The right vial displays how catalyst **2** precipitates into a powder in the presence of water.

Sample	Catalyst	Average TON	Average mmol H2/ g gel
PMI-SA[2.5]	1	8000 (±1630)	0.30 (±0.078)
PMI-SA[2.5]	2	15400 (±2160)	0.55 (±0.065)
PMI-SA[2.5]	3	142 (±28)	0.054 (±0.010)
PMI-SA[2.5]	4	2.6 (0.6)	0.039 (±0.0086)
PMI-PDDA	1	5040 (±609)	N/A
PMI-PDDA	2	11100 (±2060)	N/A
PMI-PDDA	3	314 (±58.9)	N/A
PMI-PDDA	4	13 (±2.2)	N/A
Ru(bpy)3	1	506 (±56)	N/A
Ru(bpy)3	2	911 (±135)	N/A
Ru(bpy)3	3	672 (±99)	N/A
Ru(bpy)3	4	86 (±7)	N/A

Table S1. Summary of HER photocatalysis results from various conditions and with catalysts **1**–**4** after irradiation for 18 hours. PMI-SA[2.5] gels are extruded from a 0.191 mm diameter nozzle.

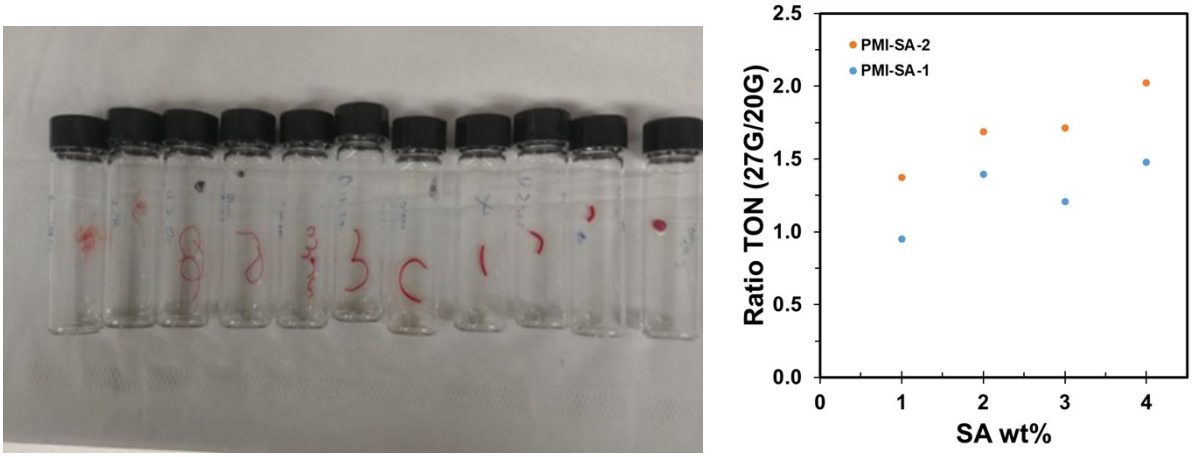

Fig. S7. PMI-SA-2.5 extruded into 0.5 M $CaCl_2$ from different nozzle diameters. From left to right 0.191 mm, 0.241 mm, 0.318 mm, 0.394 mm, 0495 mm, 0.584 mm, 0.838 mm, 1.194 mm, 1.372 mm, 1.6 mm, and bulk blob. Plot of the ratio between the TON with the 27G (0.191 mm) and 20G (0.584 mm) samples at varying SA loadings. PMI-SA-**1** and PMI-SA-**2** were prepared with SA loading between 1 wt% and 4 wt% and each ink was extruded through a 27G nozzle (0.191 mm) or a 20G nozzle (0.584 mm). For instance, PMI-SA-1 shows a ratio of 1 at 1wt% loading, indicating that the diffusivity of SA is high enough that the HER is not affected by a reduction of gel diameter. However, the ratio increases with higher SA loading indicating that slower diffusion enhances the effect of decreasing gel diameter.

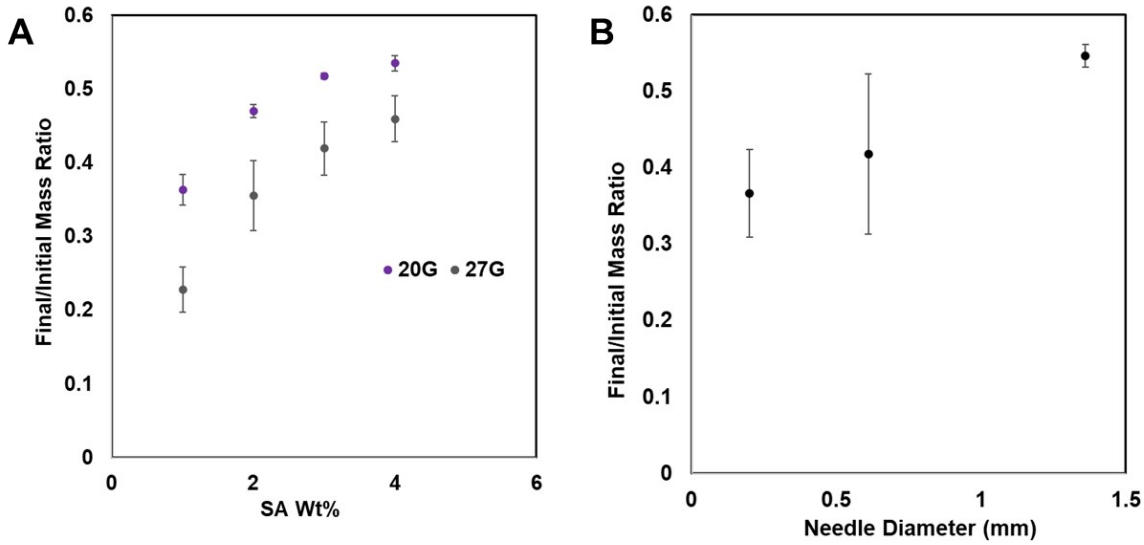

Fig. S8. (A) Ratio of final mass of measured pure SA gel to the initial mass of the ink before gelation as a function of SA loading. The 20G title represents gels extruded from a 0.584 mm diameter nozzle and the 27G title represents gels extruded from a 0.191 mm diameter nozzle. (B) Ratio of final mass of measured pure SA gel to the initial mass of the ink before gelation as a function of needle extrusion diameter for a SA[2.5] ink.

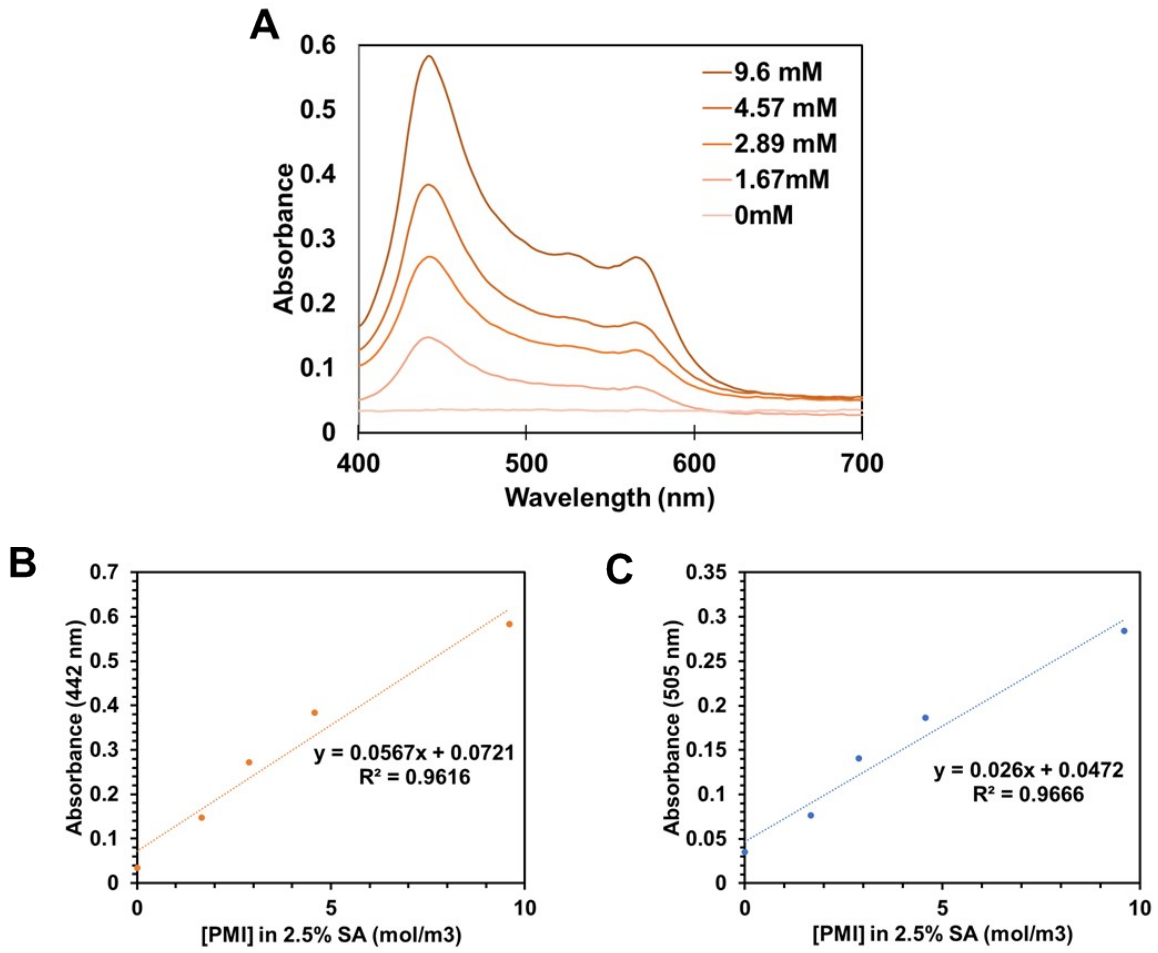

Fig. S9. (A) UV-Vis spectra of ungelled 2.5 wt% SA solution containing different concentrations of PMI. Inks were thoroughly mixed and bubbles were removed before measurement and spectra were taken against a baseline of water. These measurements were taken using a 0.05 mm quartz sandwich cuvette. The absorbance values at (B) 442 nm and (C) 505 nm were plotted against the concentration of PMI to determine the molar attenuation coefficients of PMI in 2.5 wt% SA. The calculated molar attenuation coefficients for PMI-SA[2.5] were 52000 m^2/mol at 505 nm and 4940 m^2/mol at 567 nm.

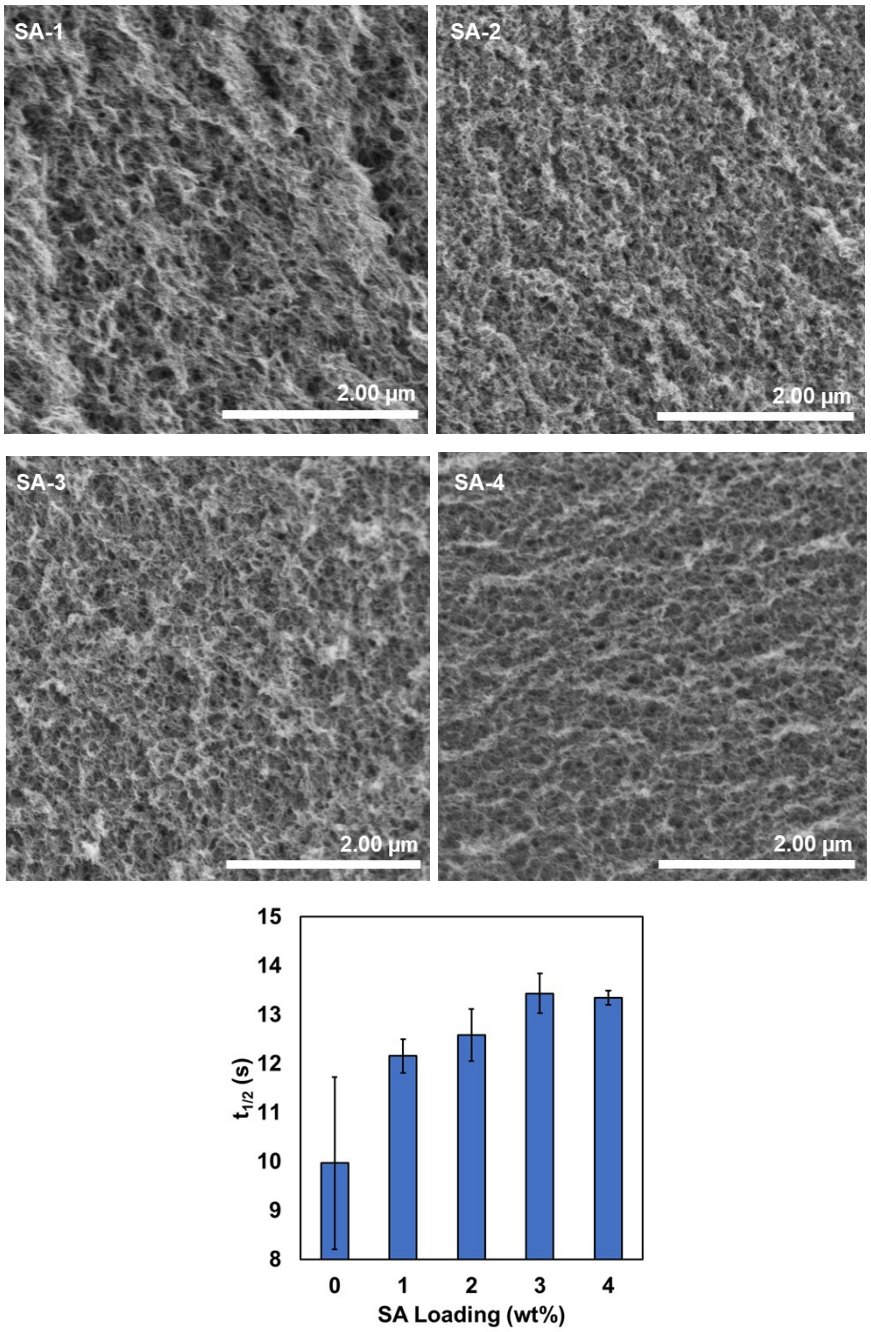

Fig. S10. SEM images of SA gels without PMI prepared by critical point drying. The SA-1 (1 wt% SA) sample is more porous than higher SA loading gels. Fluorescence Recovery After Photobleaching (FRAP) measurement of $t_{1/2}$ for SA gels of different SA wt%. Measurements were made using fluorescein as a bleachable dye. The high variability in the fluorescein solution (0% SA) results from the convection of the solution in the well plate. The results of FRAP show the half-life recovery of the dye to increase with increasing SA loading up to 3 wt% where the half-life plateaus.

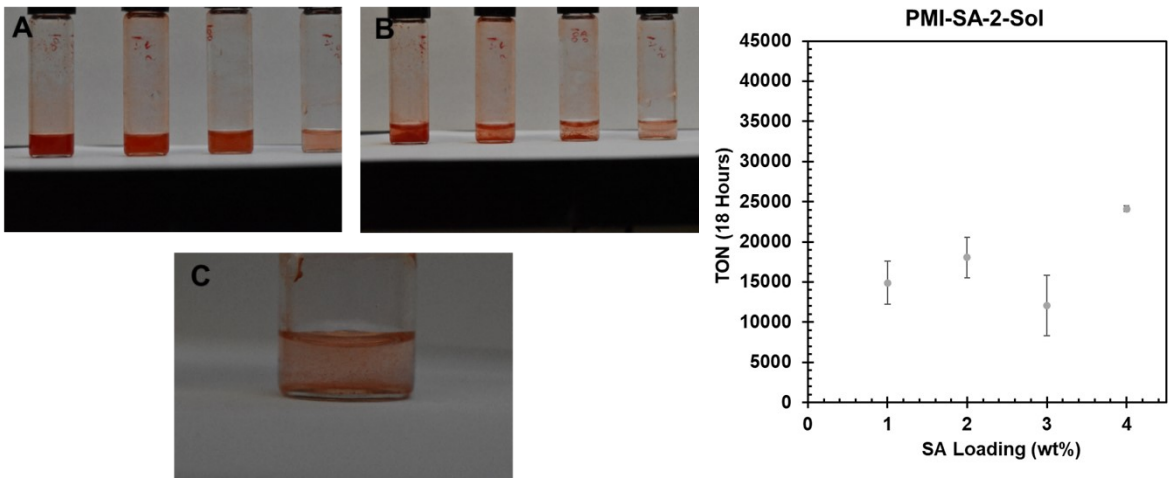

Fig. S11. Photographs of (A) fully dispersed ungelled PMI-SA in AA catalysis solution without $CaCl_2$. From left to right vials contain 100 mg of ink, 75 mg of ink, 50 mg of ink, and 25 mg of ink. (B) After one day, the ungelled samples settled out of solution as a fluffy precipitate that could be redispersed with vortex mixing. (C) Small precipitates of ungelled PMI-SA in catalysis solution were visible in the low concentration solution. (D) HER TON after 18 hours of illumination for PMI-SA[X]-2 ink with various SA loadings extruded into AA solution without $CaCl_2$. These PMI-SA samples were vortexed to achieve good dispersion and represent the fastest possible diffusion for a PMI-SA[X]-2 sample. There is a general positive trend for HER as SA loading is increased.

Sample	Cycle	Average TON	TON SD	mmol H2/g gel	mmol H2/g gel SD
PMI-SA[2.5]-1	1	3876	299	1.36E-01	1.0E-02
	2	2347	282	8.21E-02	9.9E-03
	3	1915	526	7.02E-02	2.0E-02
	4	1060	223	3.84E-02	8.3E-03
	5	911	125	3.14E-02	5.4E-03
	6	805	103	2.10E-02	1.4E-02
PMI-SA[2.5]-2	1	13704	1939	5.02E-01	7.1E-02
	2	15656	1635	5.73E-01	6.0E-02
	3	13501	1931	4.94E-01	7.1E-02
	4	12044	2809	4.41E-01	1.0E-01
	5	7142	1917	2.62E-01	7.0E-02
	6	4644	1427	1.70E-01	5.2E-02
PMI-SA[2.5]-3	1	148.46	28.01	4.97E-02	9.4E-03
	2	145.78	19.24	4.73E-02	6.9E-03
	3	99.50	4.45	3.29E-02	1.6E-03
	4	84.15	6.16	2.77E-02	2.2E-03
	5	57.53	17.04	1.93E-02	5.7E-03
	6	42.94	7.29	1.44E-02	2.4E-03
PMI-SA[2.5]-4	1	1.15	0.27	2.13E-02	4.9E-03
	2	1.55	0.20	2.51E-02	6.7E-03
	3	1.36	0.22	1.79E-02	3.3E-03
	4	1.34	0.21	1.54E-02	3.2E-03
	5	1.32	0.17	2.22E-02	2.8E-03
	6	1.32	0.19	1.96E-02	3.6E-03

Table S2. TON and HER generation for PMI-SA[2.5] samples used in long-term reusability studies

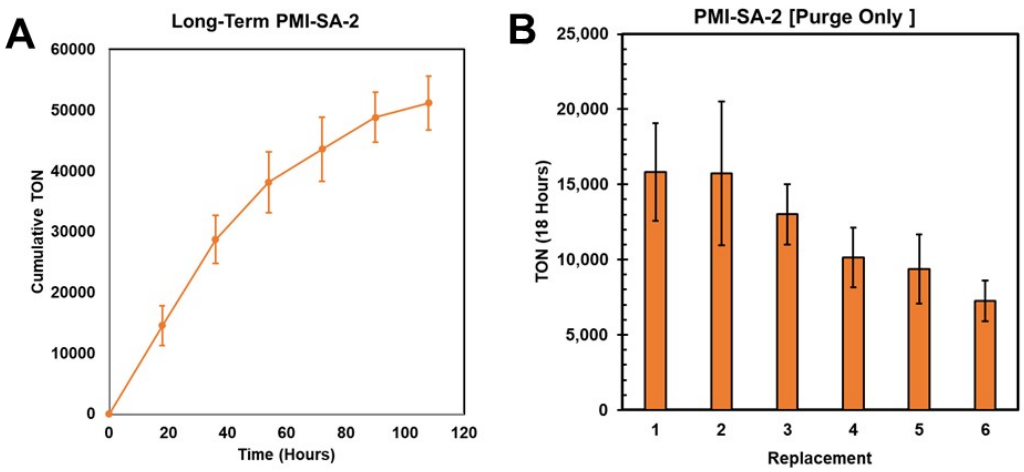

Fig. S12. (A) Plot of cumulative TON for PMI-SA[2.5]-2 (0.191 mm) over 108 hours. HER begins to noticeably decline after 40 hours of light exposure. (B) PMI-SA[2.5]-2 (0.191 mm) samples were kept in the same AA solution and purged after headspace measurement.

Sample	Needle Gauge	Light exposure	Storage Time	Average TON	TON SD
		Hours	Days		
PMI-SA-2	27G	18	0	13704	1939
PMI-SA-2	27G	18	7	16858	4307
PMI-SA-3	27G	18	0	148.46	28.01
PMI-SA-3	27G	18	7	43.78	14.90
PMI-SA-4	27G	18	0	1.15	0.27
PMI-SA-4	27G	18	7	0.99	0.51

Table S3. HER values for PMI-SA[2.5] (0.191 mm) after being stored for one week in deionized water under atmospheric conditions. HER values from fresh samples from the same batch were included for comparison. The needle gauge 27G represents a extrusion diameter of 0.191 mm.

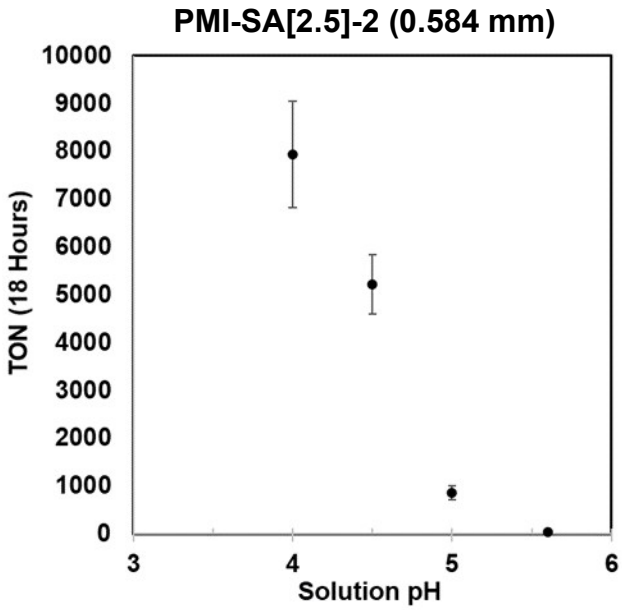

Fig. S13. Photocatalysis for PMI-SA[2.5]-**2** gel extruded from a 0.584 mm nozzle in AA solution adjusted to different pH. As the solution pH is increased above 4, HER diminishes to nearly zero at pH 5.6. At pH 6, no H_2 was measured in the catalysis headspace. We attribute this to the limitation of AA as a sacrificial electron donor and the decrease in available protons for HER. pH 4 is near the pK_a of AA, indicating a maximum in available protons and soluble ascorbate.

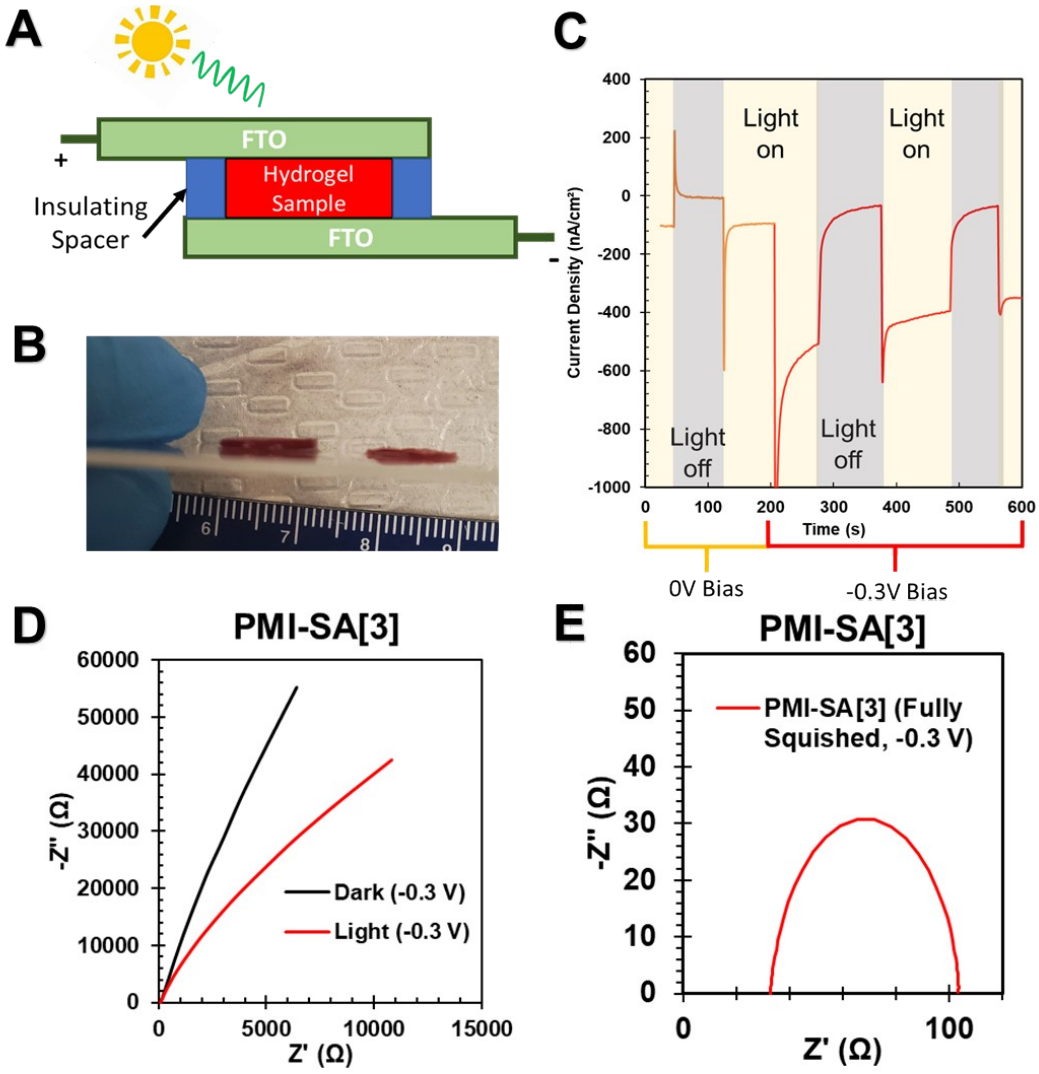

Fig. S14. Hydrogel conductivity measurements of 1.0 mm thick PMI-SA[3] gels. Samples were soaked in deionized water ionic current contribution. (A) Measurements used a two-electrode setup where gels were sandwiched between FTO substrates separated by 0.13 mm thick insulating spacers, (B) resulting in gels being compressed. (C) Chronoamperometry measured under both dark and illuminated conditions at 0 V bias and -0.3 V bias. Under both biases, the illuminated condition displayed a higher conductivity relative to the dark condition, indicating photoconductivity. Some residual ionic conductivity remained as evidenced by transient current. The illuminated PMI-SA[3] gel showed a resistivity of around 33 MΩ*cm. (D) EIS measurements at -0.3 V bias also indicated photoconductivity and a large electrical resistance. (E) However, when EIS was performed without a spacer and gels were fully compressed to a thickness of 0.075 mm, an electrical conductivity of 0.17 mS/cm was achieved in the dark. This measurement demonstrates the intrinsic conductivity of PMI assemblies.

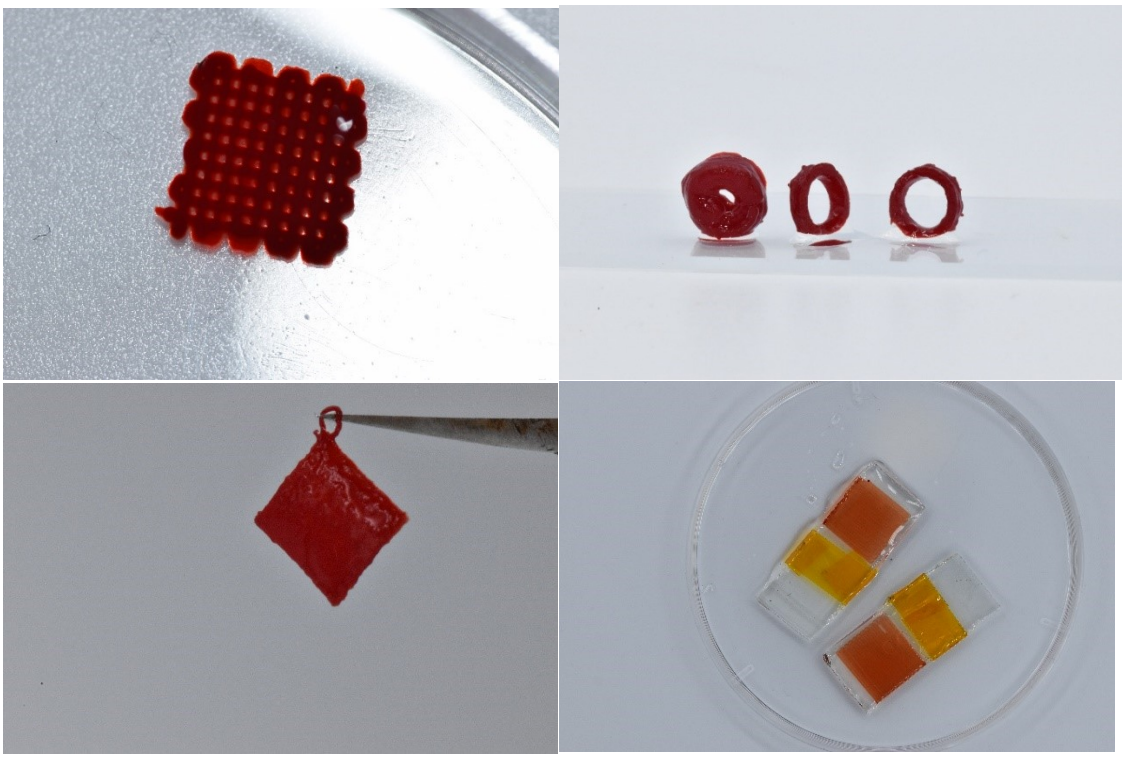

Fig. S15. 3D-printed PMI-SA[3] gels in various shapes and structures.

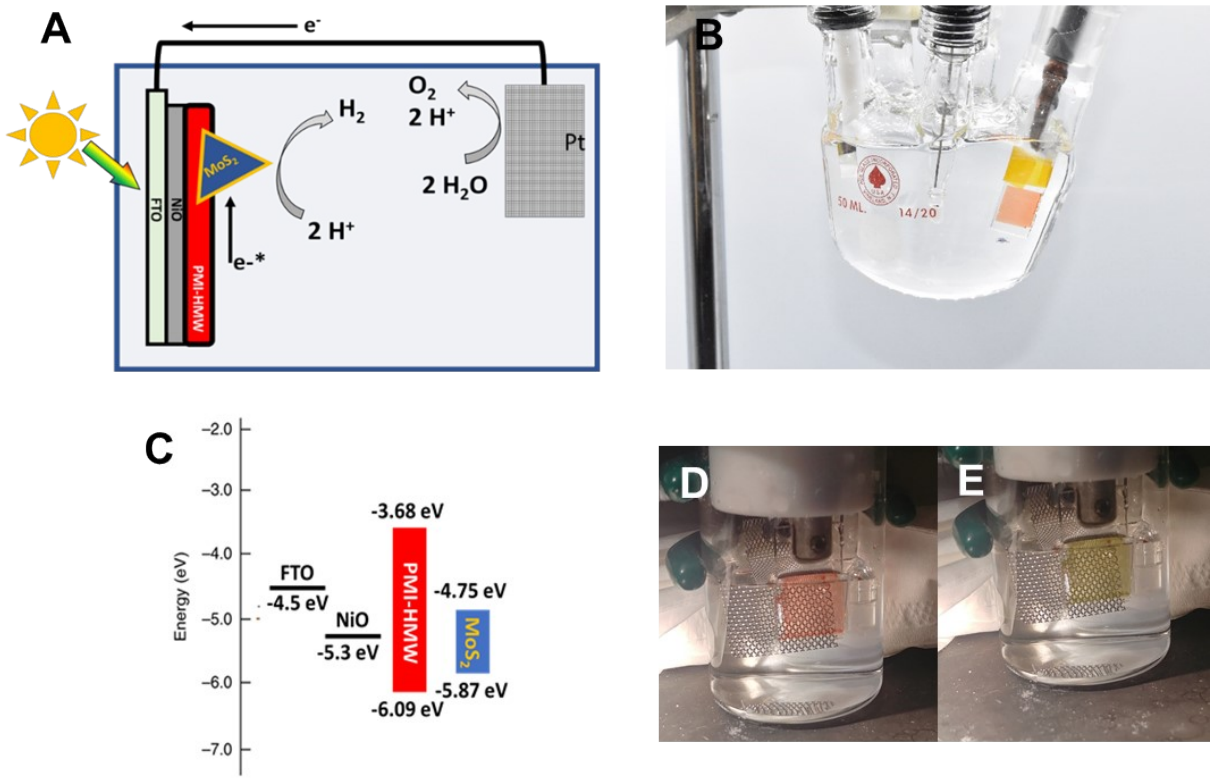

Fig. S16. (A) Schematic of PMI-SA electrode setup for HER. (B) Photograph of electrochemical setup. Samples are referenced to a Ag/AgCl 3M NaCl reference electrode. (C) energy levels of the designed photocathode (D) An electrode composed of PMI-SA[3] printed on bare FTO in a 0.5 M H_2SO_4 and begins to turn green (E) exposed to voltage more negative than -0.98 V vs AgCl. This color change is indicative of a direct electron injection into the LUMO of PMI. The fact that the color change is uniform throughout the entire gel indicates electronic connection between the gel and the electrode beyond their physical contact.

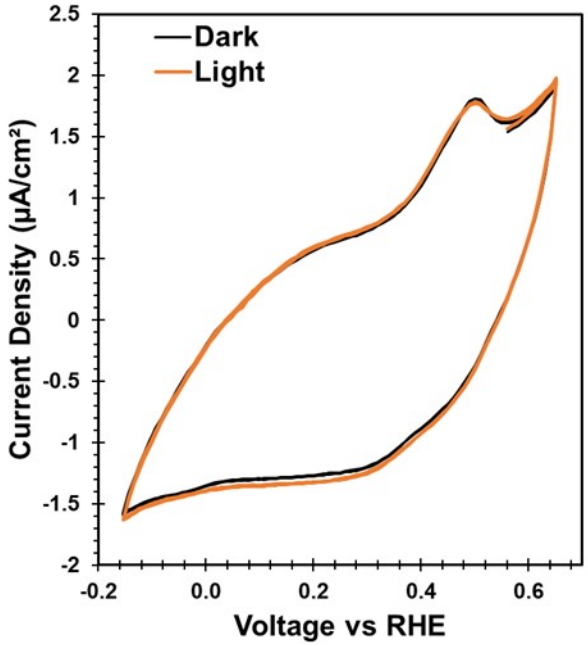

Fig. S17. CV of bare FTO-NiO substrate under typical photocatalysis conditions. When illuminated, the electrode substrate produces a maximum of 0.06 μA/cm^2 of photocurrent.

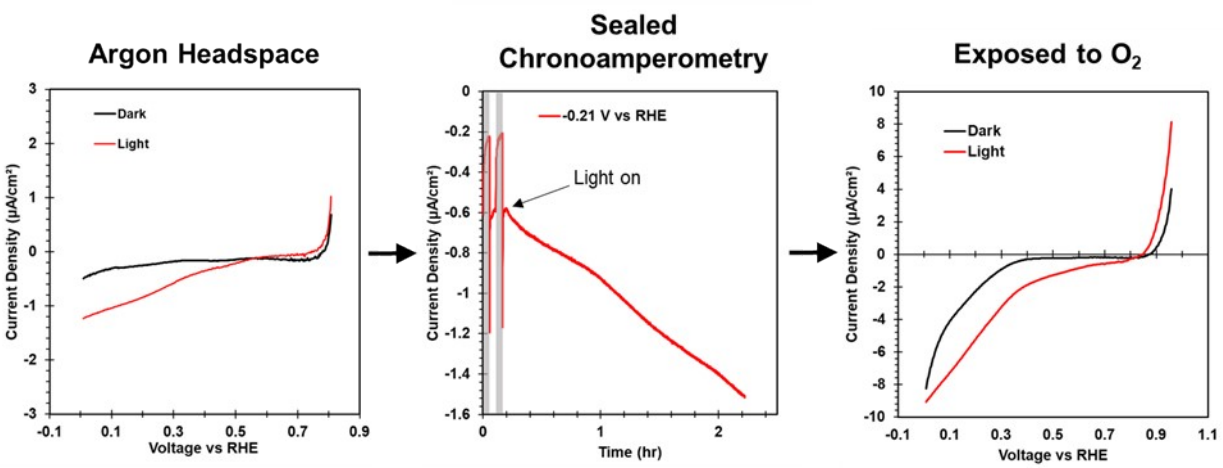

Fig. S18. PMI-SA[3]-**4** electrode devices before (Left) chronoamperometry and after chronoamperometry (Right). (Middle) Chronoamperometry was performed in pH 6 buffer electrolyte in a sealed electrochemical cell purged with Ar. Over the course of the measurement, oxygen infiltrated the electrochemical cell. The resulting increase in current was the result of oxygen reduction into H_2O_2, which was later confirmed by a colorimetric assay. The concentration of H_2O_2 was relatively low, which is likely the result of SA oxidation by H_2O_2. Purging the cell with Ar after chronoamperometry returned the electrochemical behavior to its initial state.

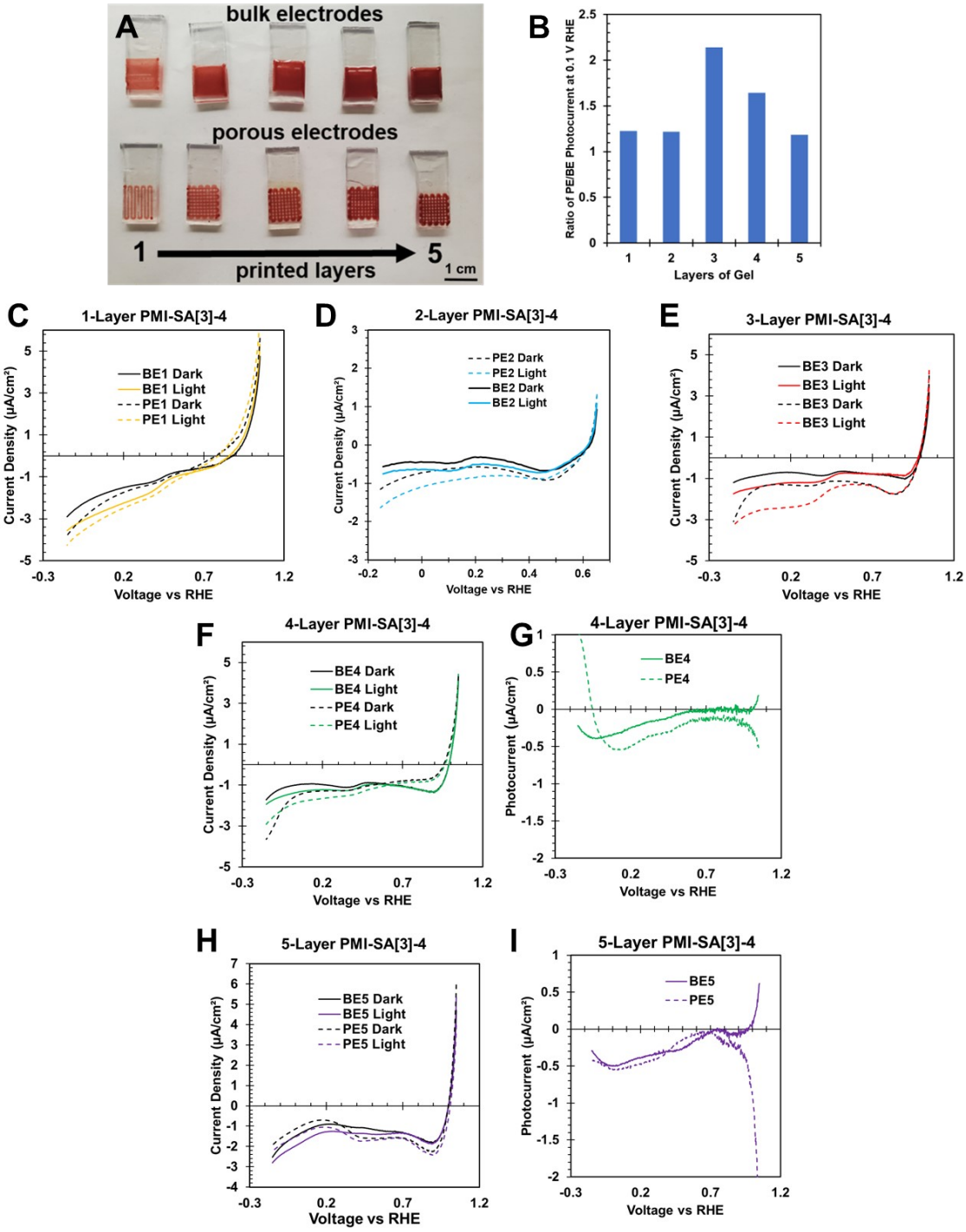

Fig. S19. (A) Image of PMI-SA[3]-**4** printed as non-porous (BE) and porous (PE) structures with thicknesses of one to five layers. (B) Ratio of photocurrent values taken from PE electrodes and BE electrodes at the same layer thickness at +0.1 V vs RHE. LSV curves of BE and PE devices with 1 layer (C), 2 layers (D), 3 layers (E), 4 layers (F), and 5 layers (H). Photocurrent values for BE4 and PE4 are plotted in image G and image I respectively.

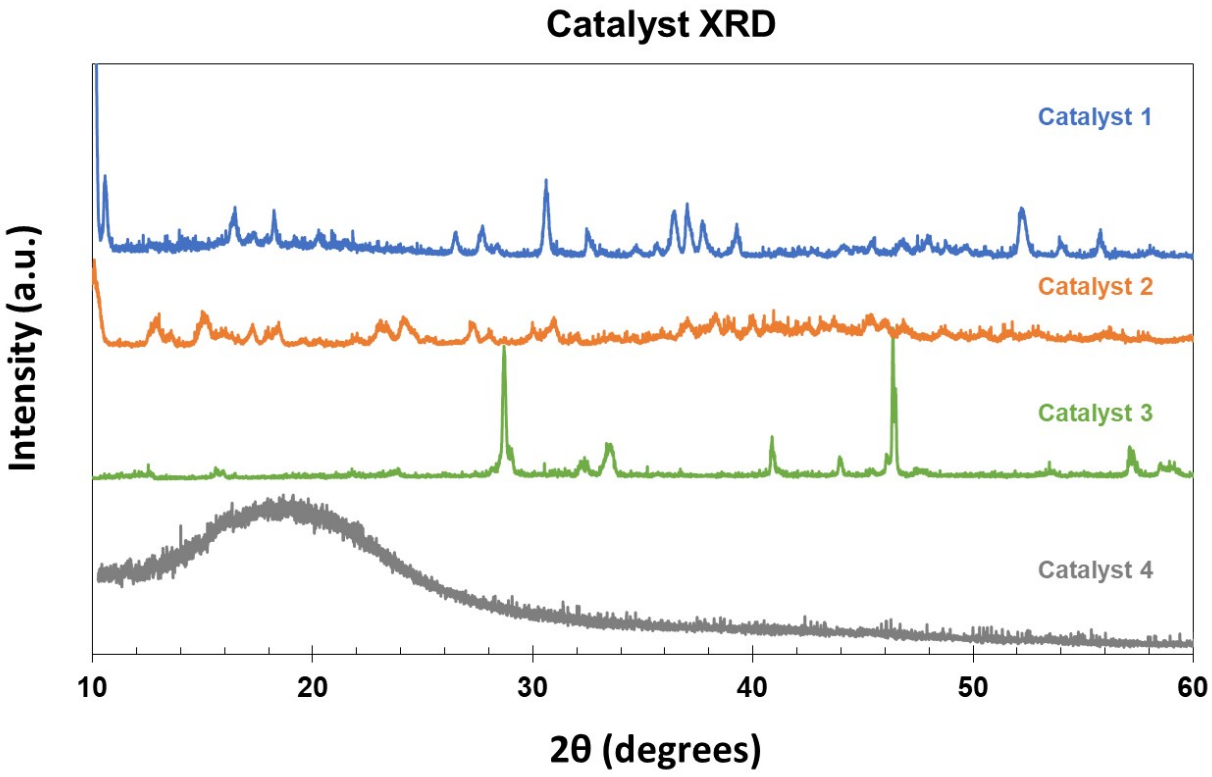

Fig. S20: XRD patterns of solid catalyst **1**, **2**, **3**, and **4.** Catalyst **1** XRD pattern reference is JCPDS 76-2038.[1] Catalyst **2** XRD pattern reference is JCPDS 631_0m_a.[2] Catalyst **3** XRD pattern reference is JCPDS is 82-1709.[9] Catalyst **4** is an amorphous powder with a broad peak centered at $2\theta=19^{o}$, which is slightly higher than typically seen in literature values.[4]

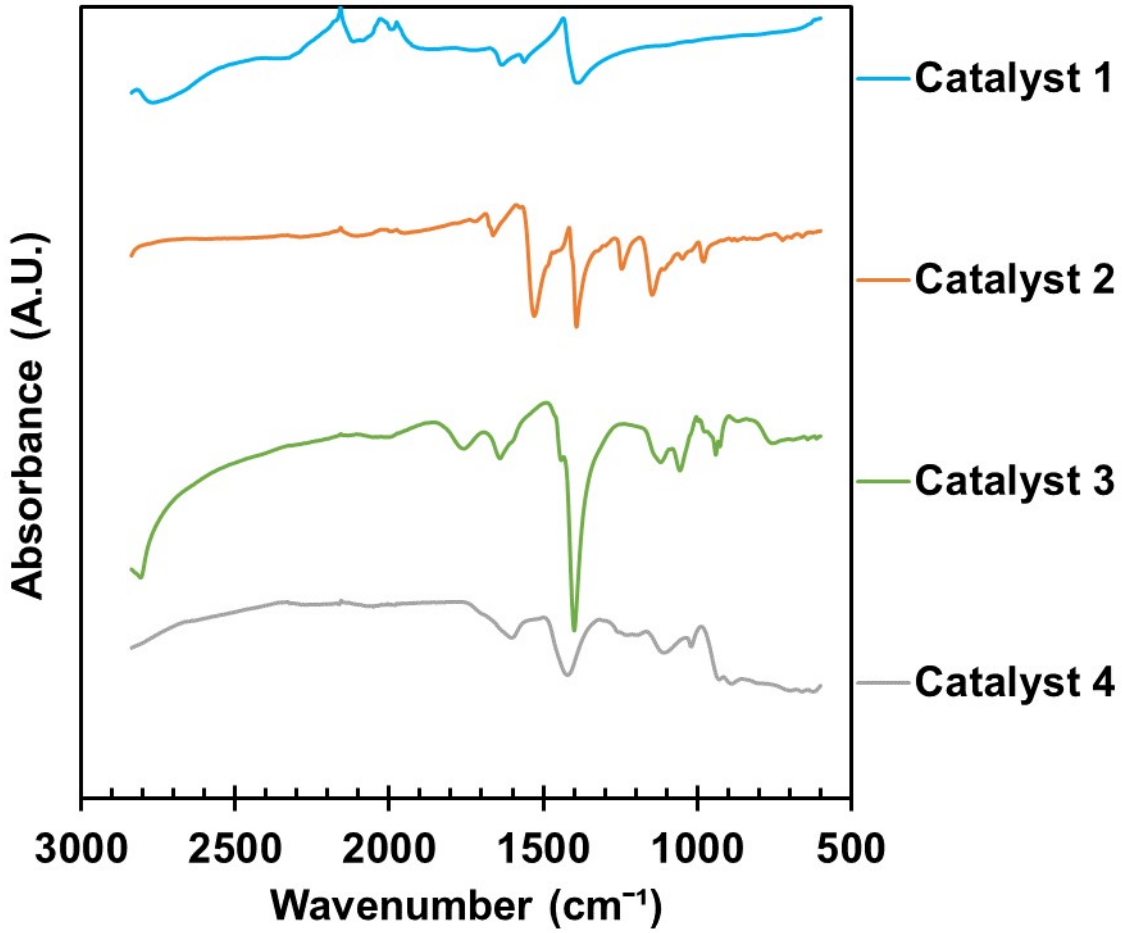

Fig. S21: IR absorption spectra of solid catalysts **1**, **2**, **3**, and **4**. For catalyst **2**, two peaks at 1240 cm^{-1} and 1140 cm^{-1} in the amine region likely corresponding to the methyl amine groups in the dithiocarbamate ligands. The peak at 1520 cm^{-1} for catalyst **2** likely corresponds to C=S.

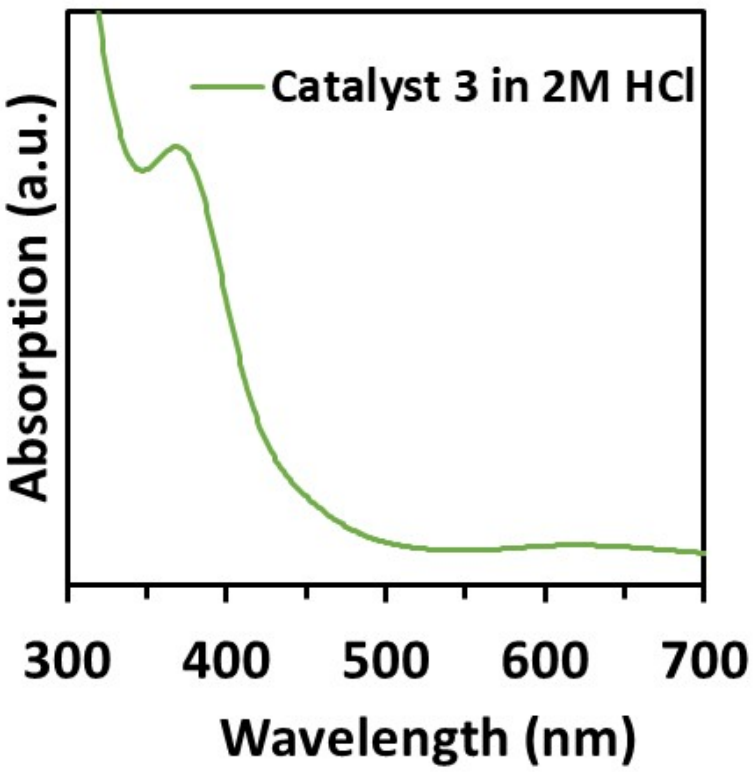

Fig. S22: (A) UV-Vis absorption spectra of catalyst **3** in 2M HCl displaying the characteristic absorption peaks around 366 nm and 603 nm.[10-11]

References

1. Kibsgaard, J.; Jaramillo, T. F.; Besenbacher, F., Building an appropriate active-site motif into a hydrogen-evolution catalyst with thiomolybdate [Mo3S13]2− clusters. *Nature Chemistry* **2014,** *6*, 248.
2. Fontenot, P. R.; Shan, B.; Wang, B.; Simpson, S.; Ragunathan, G.; Greene, A. F.; Obanda, A.; Hunt, L. A.; Hammer, N. I.; Webster, C. E.; Mague, J. T.; Schmehl, R. H.; Donahue, J. P., Photocatalytic H2-Evolution by Homogeneous Molybdenum Sulfide Clusters Supported by Dithiocarbamate Ligands. *Inorganic Chemistry* **2019,** *58* (24), 16458-16474.
3. Shibahara, T.; Yamasaki, M.; Sakane, G.; Minami, K.; Yabuki, T.; Ichimura, A., Syntheses and electrochemistry of incomplete cubane-type clusters with M3S4 cores (M = molybdenum, tungsten). X-ray structures of [W3S4(H2O)9](CH3C6H4SO3)4.cntdot.9H2O, Na2[W3S4(Hnta)3].cntdot.5H2O, and (bpyH)5[W3S4(NCS)9].cntdot.3H2O. *Inorganic Chemistry* **1992,** *31* (4), 640-647.
4. Lee, C.-H.; Lee, S.; Lee, Y.-K.; Jung, Y. C.; Ko, Y.-I.; Lee, D. C.; Joh, H.-I., Understanding the Origin of Formation and Active Sites for Thiomolybdate [Mo3S13]2– Clusters as Hydrogen Evolution Catalyst through the Selective Control of Sulfur Atoms. *ACS Catalysis* **2018,** *8* (6), 5221-5227.
5. Ho, P.; Thogiti, S.; Bao, L. Q.; Cheruku, R.; Ahn, K.-S.; Hong Kim, J., Enhanced efficiency via blocking layers at photocathode interfaces in cobalt-mediated tandem dye-sensitized solar cells. *Solar Energy* **2018,** *161*, 9-16.
6. Weingarten, A. S.; Kazantsev, R. V.; Palmer, L. C.; McClendon, M.; Koltonow, A. R.; Samuel, A. P. S.; Kiebala, D. J.; Wasielewski, M. R.; Stupp, S. I., Self-assembling hydrogel scaffolds for photocatalytic hydrogen production. *Nature Chemistry* **2014,** *6*, 964.
7. Hestand, N. J.; Kazantsev, R. V.; Weingarten, A. S.; Palmer, L. C.; Stupp, S. I.; Spano, F. C., Extended-Charge-Transfer Excitons in Crystalline Supramolecular Photocatalytic Scaffolds. *Journal of the American Chemical Society* **2016,** *138* (36), 11762-11774.
8. Dannenhoffer, A. J.; Sai, H.; Harutyunyan, B.; Narayanan, A.; Powers-Riggs, N. E.; Edelbrock, A. N.; Passarelli, J. V.; Weigand, S. J.; Wasielewski, M. R.; Bedzyk, M. J.; Palmer, L. C.; Stupp, S. I., Growth of Extra-Large Chromophore Supramolecular Polymers for Enhanced Hydrogen Production. *Nano Letters* **2021,** *21* (9), 3745-3752.
9. Gayathri, V.; Isaqu, J.; Raja Mohan, C., Graphene Quantum Dots Supported Mo3S4 as a Promising Candidate for Pt-Free Counter Electrode in Dye-Sensitized Solar Cell and Supercapacitor Applications. *ECS Journal of Solid State Science and Technology* **2021,** *10*.
10. Click, K. A.; Beauchamp, D. R.; Huang, Z.; Chen, W.; Wu, Y., Membrane-Inspired Acidically Stable Dye-Sensitized Photocathode for Solar Fuel Production. *Journal of the American Chemical Society* **2016,** *138* (4), 1174-1179.
11. N. Sokolov, M.; Coichev, N.; D. Moya, H.; Hernandez-Molina, R.; D. Borman, C.; Geoffrey Sykes, A., New procedures for the preparation of [Mo3S4(H2O)9]4+, [Mo4S4(H2O)12]5+ and [Mo7S8(H2O)18]8+ and their Se analogues: redox and substitution studies on the double cube [Mo7S8(H2O)18]8+ *Journal of the Chemical Society, Dalton Transactions* **1997,** (11), 1863-1870.